Measurements of Rotordynamic Force Coefficients of Metallic Type Brush Seals

Pascal Jolly[1(✉)], Olivier Bonneau[1], Mihai Arghir[1], Florent Cochain[2], and Jérôme Dehouve[3]

[1] Institut Pprime, CNRS - Université de Poitiers - ISAE ENSMA, Chasseneuil du Poitou, France
pascal.jolly@univ-poitiers.fr
[2] Ariane Group, Vernon, France
[3] CNES, DLA, Paris, France

Abstract. The present paper presents experimental measurements of rotordynamic force coefficients for a multistage arrangement of four identical brush seals. The bristles are metallic, with a lay angle of 50° from radial centerline and have an initial radial interference with the shaft of 0.12 mm. According to a radial feeding groove, two pairs of two seals are tested face to face. The supply pressures are 0.54, 0.82, 1.1, 1.75 and 2.4 MPa, with a discharge pressure of 0.4 MPa. The working fluid is water. The rotor is centered and the operating spinning speeds are 50, 3000 and 6000 rpm. For given working conditions (supply pressure and rotor speed), a set of dynamic excitations (two directions and 8 frequencies), imposed to the rotor, provide complex impedances that are used for identifying rotordynamic force coefficients. Results are discussed in order to highlight the respective impact of rotor speed and supply pressure on brush seals performances.

Keywords: Brush seals · Rotordynamic force coefficients · Water

1 Introduction

Designing rotating shaft sealing device for turbomachinery purpose requires to optimize leakage control but also rotordynamic performances. In many cases, the straightforward solution is the use of a labyrinth seal, according to the vast amount of data and successful applications associated to this kind of seals. Considering permanent increase of rotational speeds, working pressures and temperatures, brush seals have arised as an alternative solution for gas turbine engines, turbopumps, gas compressors and steam generators [1–3]. As indicated in [4], brush seals provide, compared to labyrinth seals, several advantages: leakage can be lowered up to 50% (in addition to stable leakage characteristics over long operating periods), permanent clearance is smaller or even zero (through bristles flexibility that accommodate transient shaft excursions) and less axial space is required. This space-saving property allows designers to arrange brush seals in a

K. L. Cavalca and H. I. Weber (Eds.): IFToMM 2018, MMS 60, pp. 335–346, 2019.
https://doi.org/10.1007/978-3-319-99262-4_24

row to obtain a multistage configuration [1,5,6]. Aslan-zada et al. [7] emphasis, through a literature review, the obvious rotordynamic benefits from implementing brush seals instead of conventional labyrinth seals in turbomachinery. In [9], the authors state that the operating conditions to be considered in brush seal design are: differential pressure, radial seal interference, inlet flow temperature, type of fluid. They add that in the case of rotor excursions, cant angle (around 45°) helps reduce the contact loads, allowing bristles to bend rather than buckle. A coating on the rotor is also required in case of large radial excursions or initial preload of the bristles (negative clearance). For turbomachines of split-case design, the segmentation of the seals is neeeded. This segmentation can affect sealing performances but direct damping coefficients are increased [10]. Finally, as indicated in [8], two methods are common to manufacture brush seals, consisting in clamping vs welding the bristle pack. In this experimental work, the rotordynamic force coefficients are identified for a multistage arrangement of four identical brush seals. The results are presented for various inlet pressures and shaft rotational speeds.

2 Test Facility

The test rig BALAFRE (BAnc LAmes Fluides à haut nombre de REynolds) is dedicated to the identification of dynamic force coefficients of thin fluid film components of high speed rotating machines. These components often use a low viscosity process fluid as lubricant (in cryogenic applications for example). Therefore, the flow in the thin fluid film exhibits high Reynolds numbers. In order to reproduce experimentally these high Reynolds numbers regimes, the test rig uses hot water as lubricant (temperatures limited to 50°C), inlet pressure as high as 4.5 MPa and tested components can have a nominal diameters up to 350 mm. These conditions lead to axial and circumferential Reynolds numbers up to 10^5. The test rig is mainly composed of a test cell, an electric motor, a hydraulic system (with pumps, tanks, filters and valves) and a Programmable Logic Controller associated with DAQ device. A cross section view of the test cell is shown in Fig. 1, where the tested component (an annular seal in the present configuration) is overhung mounted at the left end of a rotating shaft 7. The rotor and the stator of the annular seal are respectively indicated as 1 and 2. This design gives a great modularity to the test cell, where various kinds of components have been mounted : seals, hydrostatic bearings and impellers.

The whole test rig is pressurized at 0.5 MPa. This means that an annular seal can have a maximum pressure difference of 4 MPa between the upstream and the downstream (discharge) chambers. The necessary flow rate (up to 120 m^3/h) is delivered by two centrifugal pumps driven by electrical motors whose total power is 330 kW. The maximum shaft speed (6000 rpm) is obtained with a three-phase asynchronous motor of 180 kW. A double conical hydrostatic thrust bearing is located close to the test component. It has many roles: first it must guide the rotation of the shaft and support the static axial load (which can reach as much as 200 kN) generated by the 4 MPa pressure difference between the two faces of

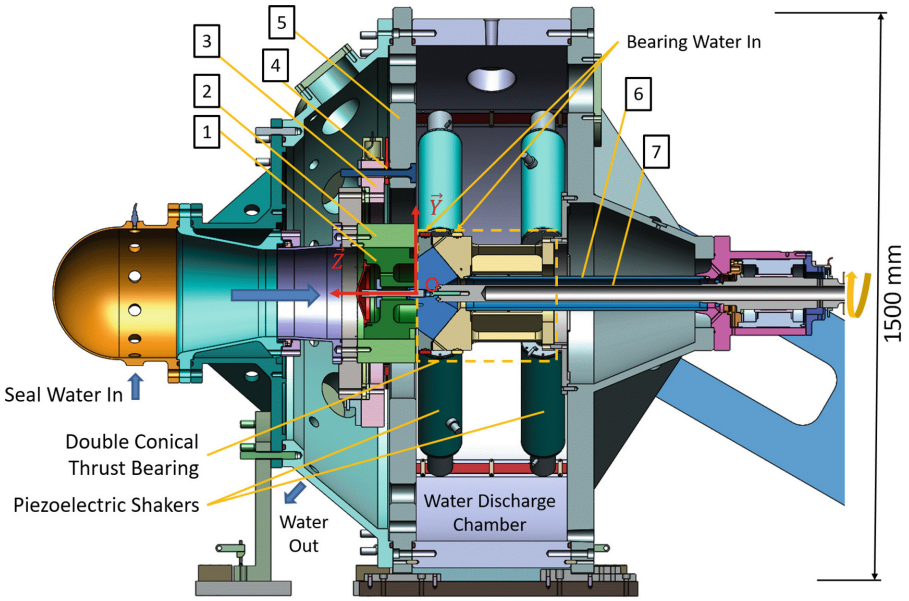

Fig. 1. Cross sectional view of the test cell - annular seal configuration

the annular seal. Its second role is to transmit the excitations imposed by the 8 piezoelectric actuators mounted four by four along two planes. The housing of the bearing is linked to the frame via a hollow tube 6 designed to be very stiff axially and flexible in the radial direction. The first natural frequency of the bending mode of the shaft is 460 Hz; the two first natural frequencies of the torsional modes are 14 Hz and 269 Hz. The double conical hydrostatic thrust bearing is provided with 2×6 recesses and orifice restrictors [11] and is fed with water at 15 MPa. The average fluid film thickness in the two parts of the bearing is about 40 µm and the axial and radial stiffnesses[1] are larger than 10^9 N/m. The outlet flow from both the tested component and the double conical hydrostatic thrust bearing is discharged in the test rig and then returns to a water tank of 5 m^3 via several hoses and pipes. Dynamic displacements are applied to the rotor by 8 piezoelectric shakers, mounted 4 by 4 in the forward and in the rear plane of the double conical hybrid bearing. The maximum dynamic displacements are ±100 µm with a frequency range from 20 to 200 Hz, corresponding to dynamic loads of 20 kN per axis[2]. The housing 2 of the tested component is fixed on a rigid part 3 which is mounted on the test rig's frame 5 via three piezoelectric

[1] The stiffnesses of the double conical hydrostatic thrust bearing are high contrary to those of the tested component in order to lower the power of the shakers.

[2] The power of the shakers is set to a percentage of their total power. Therefore, the obtained amplitudes of displacements of the rotor depend on the direct stiffnesses of the tested component.

force transducers (Kistler 9167) [4] each one being able to measure three components, in a range $[-20\,\text{kN}; 20\,\text{kN}]$. Their stiffnesses are respectively $4.6 \times 10^9\,\text{N/m}$ and $1.67 \times 10^9\,\text{N/m}$ in directions **Z** and **X**, **Y**. For each axis, the proportional error is $\leq \pm 1\,\%$ and the hysteresis is $\leq 2\,\%$, both for the full scale output. The three sensors constitute a force balance. The first natural frequency of the axial mode of the stator assembly (housing and force sensors) is 280 Hz. The two first natural frequencies of the bending mode are 370 Hz and 520 Hz. The housing is equipped with 6 eddy current proximity probes (Bently Nevada 3300 XL 8 mm), positioned three by three in the front and rear plane (for an annular seal or a hydrostatic bearing). Their linearity error is $\leq 5\,\%$. These sensors measure the relative displacements between the rotor and the housing. Therefore, the position of the rotor center in the two planes as well as the radial clearance can be deduced. Before each test, a dedicated part, having an outside diameter that fits exactly the housing's inside diameter, is used to calibrate simultaneously the response (gain and offset) of the 6 displacement sensors. Misalignment of the rotor can also be obtained knowing that the two measuring planes are equidistant from the housing midplane. Three accelerometers are also mounted on the housing enabling the measurement of its absolute movements.

3 Dynamic Coefficients Identification

The dynamic displacements of the rotor imposed by the shakers generate fluid forces that the housing transmits to the piezoelectric force transducers (acting like high stiffness springs). For lateral displacements of the rotor along **X** and **Y** axes of the coordinate system defined in Fig. 1, the equations of the fundamental principle of dynamics applied to the housing with respect to the center of the component O are:

$$\begin{cases} m\ddot{x} = -f_x + \sum_{k=1}^{3} fb_x^k \\ m\ddot{y} = -f_y + \sum_{k=1}^{3} fb_y^k \end{cases} \tag{1}$$

where f and fb^k are respectively the fluid film forces and the forces measured by the k^{th} sensor of the force balance while the subscript x and y denote their directions. In order to evaluate the contribution of inertial forces in Eq. 1, the assembly stator/force balance can be likened to a single degree of freedom spring (of stiffness K) - mass (M) system subjected to a harmonic force $f(t)) = f_0 sin(\omega t)$. The equation of motion of this system is $M\ddot{x} + Kx = f(t)$ and the solution is $x(t) = \frac{f_0}{K} \frac{\omega_0^2}{\omega_0^2 - \omega^2} sin(\omega t)$, where $\omega_0 = \sqrt{\frac{K}{M}}$ is the natural frequency of the system. According to the ratio $\frac{M\ddot{x}}{Kx} = \frac{M\omega^2}{K}$, with $M = 250\,\text{kg}$ and $K = 3 * 1.67 \times 10^9\,\text{N/m}$, the contribution of inertial forces can be calculated in respect of excitation frequency ω. As shown in Fig. 2, inertial forces represent 1.7% of the total measured forces at $\omega = 90\,\text{Hz}$ and 3% at $\omega = 120\,\text{Hz}$.

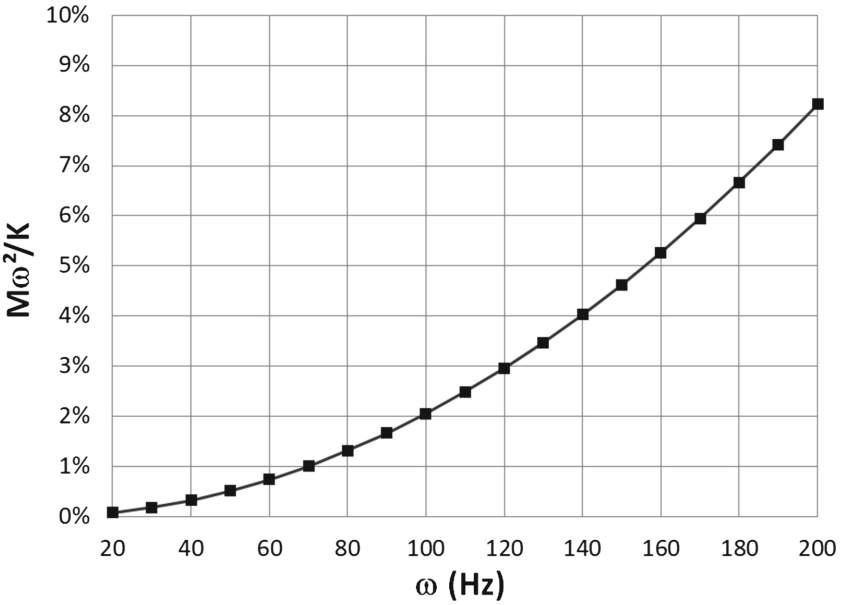

Fig. 2. Inertial forces contribution in the total measured forces in respect of excitation frequency at ω

For an excitation frequency in the range 20 to 120 Hz, the accelerations of the housing can be neglected [12], and Eq. 1 can be simplified as:

$$\begin{cases} f_x = \sum_{k=1}^{3} f b_x^k \\ f_y = \sum_{k=1}^{3} f b_y^k \end{cases} \tag{2}$$

Introducing the small perturbation hypothesis, fluid film forces can be described by linear dynamic coefficients (stiffness K, damping C and added mass M) or impedances Z. In the frequency domain (after applying the Fourier transform), the fluid film forces and the displacements of the rotor are written as follows:

$$\begin{cases} F_x = Z_{xx} X + Z_{xy} Y \\ F_y = Z_{yx} X + Z_{yy} Y \end{cases} \tag{3}$$

The unknown impedances Z_{xx}, Z_{xy}, Z_{yx} and Z_{yy} are found by using two linearly independent excitations (denoted by the superscripts 1 and 2) consisting in lateral vibrations obtained by successively exciting the piezoelectric shakers in two orthogonal directions and with the same phase for the front and rear planes. The impedances are computed by inverting the displacement matrix as follows:

$$\begin{bmatrix} Z_{xx} & Z_{xy} \\ Z_{yx} & Z_{yy} \end{bmatrix} = \begin{bmatrix} F_x^1 & F_x^2 \\ F_y^1 & F_y^2 \end{bmatrix} \begin{bmatrix} X^1 & X^2 \\ Y^1 & Y^2 \end{bmatrix}^{-1} \tag{4}$$

The stiffness, damping and added mass matrices of coefficients are calculated from the real and imaginary part of the corresponding impedances as follows:

$$\begin{cases} K_{ij} - M_{ij}\omega^2 = \Re\left[Z_{ij}\left(\omega\right)\right] \\ j\omega C_{ij} = \Im\left[Z_{ij}(\omega)\right] \end{cases} \tag{5}$$

with $[ij] = [xx; xy; yx; yy]$. Equation 5 shows that in order to enable the identification of constant dynamic coefficients[3], the real part of the impedance must describe a parabola and its imaginary part must describe a straight line. In order to perform a curve fitting by the least square procedure, the impedances are calculated for a significant number of excitation frequencies ω. Examples of real and imaginary parts of the impedances used during the identification are respectively shown in Figs. 3 and 4.

The uncertainties in K_{ij} and C_{ij} are respectively estimated to $\pm 15\,\%$ and $\pm 30\,\%$.

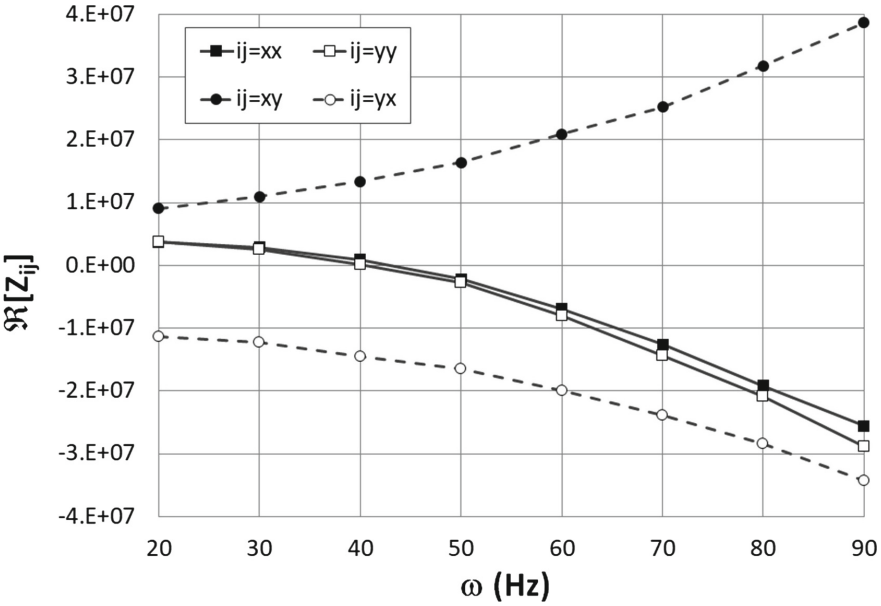

Fig. 3. Curve fitting of impedance's real parts for identification as a function of ω(Hz) in abscissa - $P_s = 1.1\,\text{MPa}$; $\Omega = 50\,\text{Hz}$

[3] As the fluid is considered as incompressible, rotordynamic coefficients are independent from the exciting frequency.

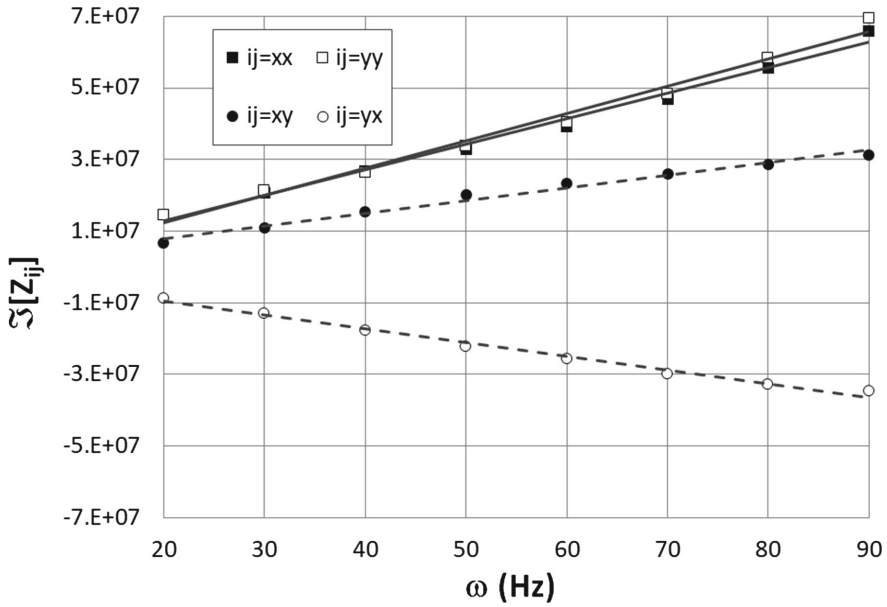

Fig. 4. Curve fitting of impedance's imaginary parts for identification as a function of ω(Hz) in abscissa - $P_s = 1.1\,\text{MPa}$; $\Omega = 50\,\text{Hz}$

4 Tested Brush Seals

Figure 5 shows the stator assembly equipped with the four brush seals (two arrangements of two identical brush seals). The fluid is introduced radially (no preswirl [5,13]), in the middle of the four seals. The process fluid is water, having an inlet temperature in the range 35 to 40.5°C and an inlet pressure up to 2.4 MPa. The seals are in one part (not segmented) with a welded design. The rotor is coated with a layer of chromium carbide. The mains seals properties are listed above[4]:

- Manufacturing design: Welded
- Plates material: 304 L Stainless Steel
- Clearance at back plate: 0.53 mm
- Front plate diameter = Back plate diameter
- Bristle diameter: 0.07 mm
- Bristle material: $HAYNES\ 25$
- Radial shaft interference: $c_0 = 0.12\,\text{mm}$
- Bristle angle: 50° lg 5°
- Bristle contact width: 2 mm
- Back plate width: 2.4 mm

[4] For confidentiality purposes, the authors are not allowed to communicate the diameter of the shaft.

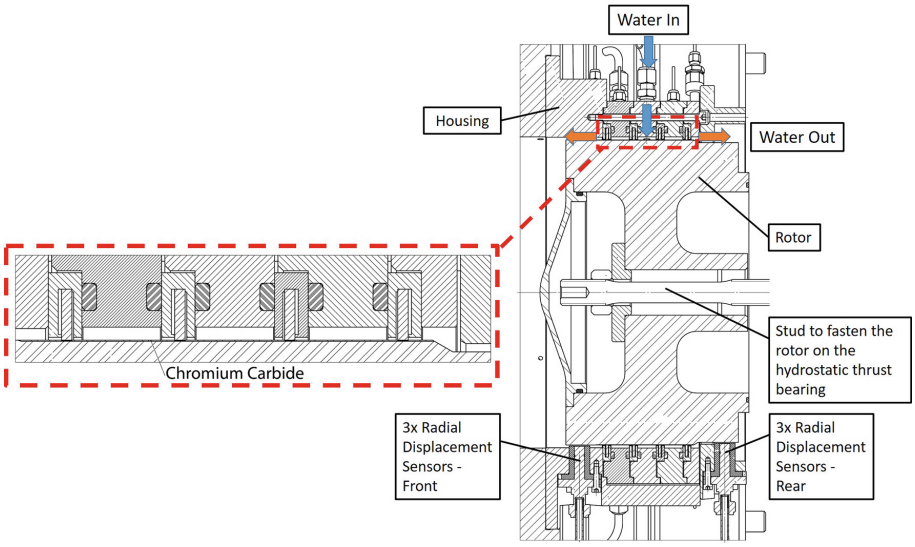

Fig. 5. Cross sectional view of the brush seals arrangement

5 Tests Conditions

All the tests have been operated with a centered position of the rotor. For each rotor speed Ω, experimental data (displacements, forces, pressures, flowrates, temperatures, torque) are recorded for steady-state static case and dynamic excitations. The tests have been performed according to the following conditions:

- Rotor speed Ω: 50, 3000 and 6000 rpm,
- Excitations frequencies ω: 20, 30, 40, 50, 60, 70, 80 and 90 Hz,
- Water supply pressure P_s: 0.54, 0.82, 1.1, 1.75 and 2.4 MPa,
- No fluid preswirl.

Figure 6 shows the unwrapped form of the inlet diameter of the stator[5], along with the four seals and the instrumentation distribution:

- 6 displacement sensors ($C11$ to $C23$),
- 15 pressure taps (P_{stat1} to P_{stat15}),
- 5 PT100 sensors (T_1 to T_5) [6],
- 3 in situ pressure sensors (P_{dyn1} to P_{dyn3}).

[5] $\mathbf{\Omega}$ is the rotating direction and Θ is the circumferential coordinate according to $\mathbf{X}$.
[6] T_B corresponds to plugged $PT100$ positions.

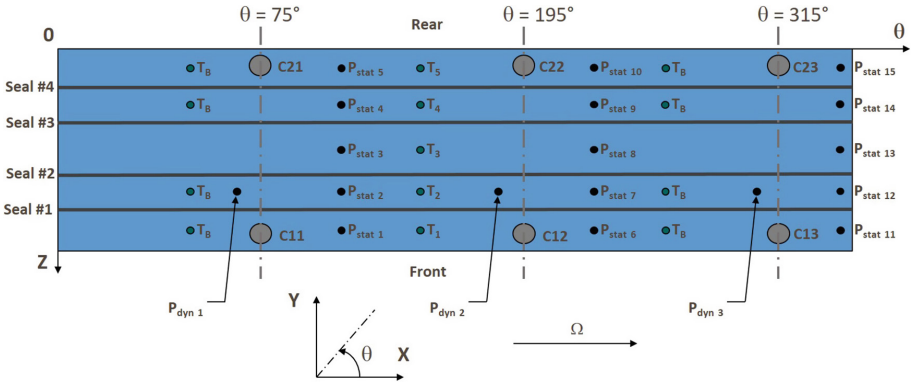

Fig. 6. Unwrapped form of the instrumented stator

6 Results and Discussion

The present experimental dynamic coefficients are made nondimensional as follows [10]:

$$\begin{cases} \text{Dimensionless stiffness coefficients} & K_{ij}^{*} = \dfrac{K_{ij} c_0}{\Delta P_{max} L_s D} \\ \text{Dimensionless damping coefficients} & C_{ij}^{*} = \dfrac{C_{ij} c_0 \Omega_{max}}{\Delta P_{max} L_s D} \end{cases} \tag{6}$$

where $\Delta P_{max} = 2.4\,\text{MPa}$ is the maximum pressure differential between the supply pressure and the discharge pressure, L_s is the sealing axial length, D is the shaft diameter, $\Omega_{max} = 100\,\text{Hz}$ is the maximum shaft speed.

Figure 7 illustrates the evolution of the direct (top) and cross-coupled (bottom) stiffness coefficients versus ΔP, for various running speed. Direct stiffness coefficients are always positive except for one case i.e. at maximum running speed and minimum pressure differential, as for an annular seals [12]. Furthermore, direct stiffness coefficients are not sensitive to Ω but increase with δP, due to the phenomenon of pressure-stiffness coupling [9]. Cross-coupled stiffness coefficients are theoretically higher at maximum shaft speed but, contrary to conventional annular seals, their values decrease with increasing ΔP, indicating the bristle packs can contribute to reduce the tangential velocity. Figure 8 illustrates the evolution of the direct (top) and cross-coupled (bottom) damping coefficients versus ΔP, for various running speed. It is interesting to note that direct damping coefficients are always positive. As for annular seals, the direct-damping coefficients are higher than the cross-coupled damping coefficient. Furthermore, damping coefficients are generally not sensitive to rotor speed, except cross-coupled damping coefficients for low differential pressure. As a final observation, present experimental stiffness and damping coefficients often satisfy

theory: for small motion about a centered position, the matrices **K**, **C** and **M** are skew-symmetric with equal entries on the main diagonal, i.e. $K_{xx} = K_{yy}$ and $K_{xy} = -K_{yx}$, etc.)

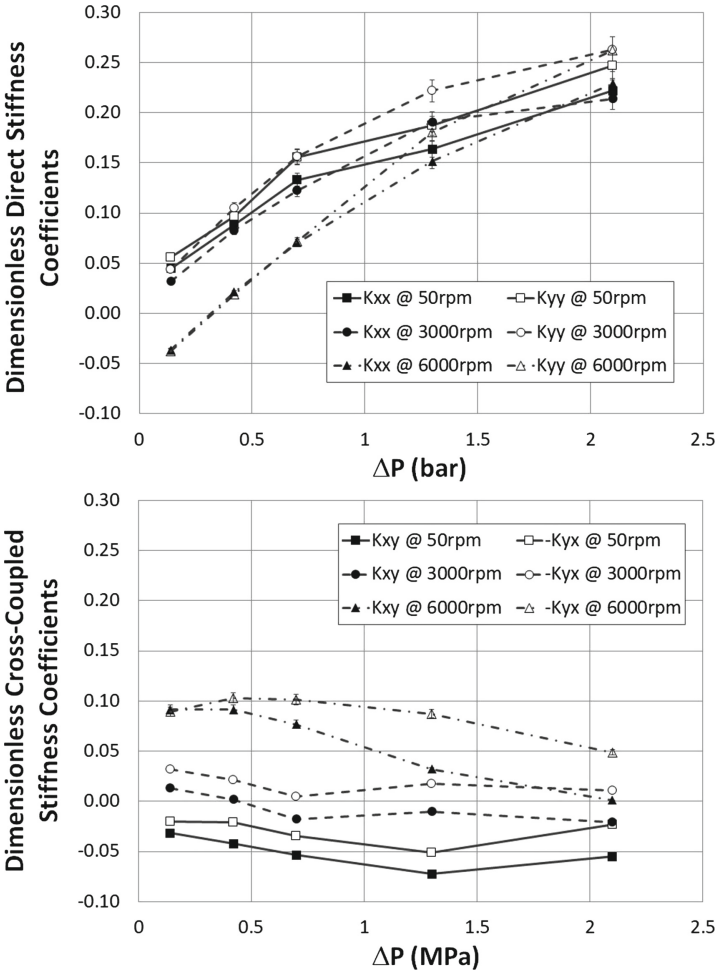

Fig. 7. Identified stiffness coefficients

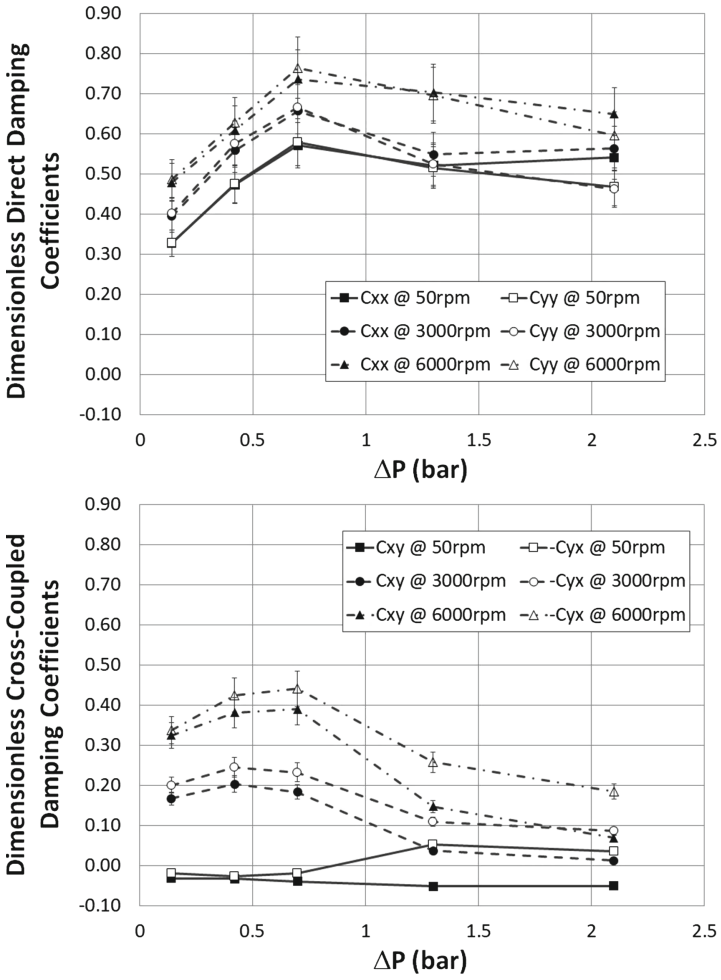

Fig. 8. Identified damping coefficients

7 Conclusion

Experimental results are presented for the direct and cross-coupled stiffness and damping coefficients for a multistage arrangement of four identical brush seals. Variable test parameters include pressure differential and shaft speed. Direct stiffness is shown to have positive value, to increase with pressure differential and to be almost the same at 3000 and 6000 rpm. Cross-coupled stiffness is generally lower than direct stiffness and is quasi-unchanged by increasing the pressure differential. Direct damping coefficients are always positive, softly dependent on shaft speed and begin to decrease after a pressure differential of 0.7 MPa.

Acknowledgements. The authors are grateful to Centre National d'Etudes Spatiales (CNES) and to ARIANE GROUP for using the test rig BALAFRE and for their agreement to present this experimental work. This work was partially funded by the French Government program "Investissements d'Avenir" (EQUIPEX GAP, reference ANR-11-EQPX-0018).

References

1. Conner, K.J., Childs, D.W.: Rotordynamic and leakage characteristics of a four-stage brush seal. Final report for period October 1988–30 August 1992. Technical report, Turbomachinery Laboratories, Texas A&M University, College Station, Texas (1992)
2. Carlile, J.A., Hendricks, R.C., Yoder, D.A.: Brush seal leakage performance with gaseous working fluids at static and low rotor speed conditions. ASME J. Eng. Gas Turbines Power **115**(2), 397–403 (1993)
3. Chupp, R.E., Holle, G.F.: Generalizing circular brush seal leakage through a randomly distributed bristle bed. ASME J. Turbomach. **118**(1), 153–161 (1996)
4. Chupp, R.E., Hendricks, R.C., Lattime, S.B., Steinetz, B.M.: Sealing in turbomachinery. J. Propul. Power **22**(2), 313–349 (2006)
5. Pugachev, A.O., Deckner, M.: Experimental and theoretical rotordynamic stiffness coefficients for a three-stage brush seal. Mech. Syst. Signal Process. **31**, 143–154 (2012)
6. Raben, M., Friedrichs, J., Flegler, J.: Brush seal frictional heat generation—test rig design and validation under steam environment. ASME J. Eng. Gas Turbines Power **139**(3), 032,502–032,502-9 (2016)
7. Aslan-zada, F.E., Mammadov, V.A., Dohnal, F.: Brush seals and labyrinth seals in gas turbine applications. Proc. IMechE Part A J. Power Energy **227**(2), 216–230 (2012)
8. Hildebrandt, M., Schwitzke, C., Bauer, H.: Experimental investigation on the influence of geometrical parameters on the frictional heat input and leakage performance of brush seals. ASME J. Eng. Gas Turbines Power (2017). https://doi.org/10.1115/1.4038767
9. Aksit, M.F.: Brush seals and common issues in brush seal applications (2012). http://research.sabanciuniv.edu/26863/1/RTO-AVT-188-KN4.pdf
10. Pugachev, A.O., Gaszner, M., Georgakis, C., Cooper, P.: Segmentation effects on brush seal leakage and rotordynamic coefficients. ASME J. Eng. Gas Turbines Power **138**(3), 032,501–032,501-9 (2015)
11. Charles, S., Bonneau, O., Frêne, J.: Determination of the discharge coefficient of a thin-walled orifice used in hydrostatic bearings. ASME J. Tribol. **127**(3), 679–684 (2005)
12. Jolly, P., Hassini, A., Arghir, M., Bonneau, O.: Experimental and theoretical rotordynamic coefficients of smooth and round-hole pattern water fed annular seals. In: Proceedings of ASME Turbo Expo 2014, Turbine Technical Conference and Exposition, 16–20 June, Düsseldorf, Germany (2014)
13. Childs, D.W., Mclean, J.E., Zhang, M., Arthur, S.P.: Rotordynamic performance of a negative-swirl brake for a tooth-on-stator labyrinth seal. ASME J. Eng. Gas Turbines Power **138**(6), 062,505–062,505-8 (2015)